International Communications in Heat and Mass Transfer 126 (2021) 105345

Contents lists available at ScienceDirect

International Communications in Heat and Mass Transfer

journal homepage: www.elsevier.com/locate/ichmt

Thermal vibrational and gravitational analysis of a hybrid aqueous suspension comprising Ag–MgO hybrid nano-additives

S.A.M. Mehryan [a], Piran Goudarzi [b], Seyed Mohsen Hashem Zadeh [c], Maryam Ghodrat [c], Obai Younis [d,e], Mohammad Ghalambaz [f,g,*]

[a] Young Researchers and Elite Club, Yasooj Branch, Islamic Azad University, Yasooj, Iran
[b] Department of Mechanical Engineering, Shahrood University of Technology, Semnan, Iran
[c] School of Engineering and Information Technology, University of New South Wales Canberra, Canberra 2610 ACT, Australia
[d] Department of Mechanical Engineering, College of Engineering at Wadi Addwaser, Prince Sattam Bin Abdulaziz University, Al-Kharj, Saudi Arabia
[e] Department of Mechanical Engineering, Faculty of Engineering, University of Khartoum, Sudan
[f] Metamaterials for Mechanical, Biomechanical and Multiphysical Applications Research Group, Ton Duc Thang University, Ho Chi Minh City, Vietnam
[g] Faculty of Applied Sciences, Ton Duc Thang University, Ho Chi Minh City, Vietnam

ARTICLE INFO

Keywords:
Thermal vibrational
Natural convection
Hybrid nanofluid
Heat transfer enhancement
Finite element method

ABSTRACT

The incorporation of simultaneous passive and active techniques for enhancing heat transfer has been a promising area of research in the last decades. As such, in the present study, thermal convection heat transfer of a hybrid nanofluid in a square cavity subjected to simultaneous effects of gravitational and vibrational forces has been addressed. Initially, the cavity, saturated with Ag-MgO hybrid nanofluid, is stagnant and in thermal equilibrium. Then, the sidewalls of the cavity are heated isothermally, and the cavity starts vibrating in a vertical direction. The upper and lower walls are kept adiabatic. Galerkin finite element method with a very small- and adaptive-time step has been used to precisely capture the impact of vibrational force on the flow and thermal fields in high frequencies. Impacts of vibration frequency, gravitational and vibration Rayleigh numbers, and the volume fraction of hybrid nano-additives are studied. It has been revealed that the external vibration amplifies the rate of heat transfer for all the studied frequencies. Moreover, although the presence of the nanoparticles seems to have a very limited effect on the effectiveness of heating, the effect of the nanoparticle concentration on the heat transfer intensity varies with time.

1. Introduction

To date, the lack of enough energy resources raises a need for researchers to investigate different heat transfer enhancement techniques. Generally, there are two distinct approaches for heat transfer enhancement, which are passive [1–4] and active techniques [5–13]. In the passive technique, no external energy or power is required, and the usage of turbulators is found to be the most effective approach in the passive technique. On the other hand, active techniques need external energy such as mechanical mixing, rotation, vibration, and addition of external electrostatic or magnetic fields [14,15].

In many engineering applications, vibration is effectively employed to enhance system efficiencies. Strengthening chemical reactions, drying, welding, and cleaning are among the numerous potential applications of vibrational oscillations [16]. One active technique that has been investigated for heat transfer enhancement by different researchers is surface vibration. This method enhances the turbulence intensity within the fluid boundary layers, which causes an enhancement in the heat transfer coefficient [17].

A large number of literature on generating enhanced heat transfer by creating adequately strong surface vibrations, especially in the natural and forced convection, have been emerged in the last two decades [15]. Much work has been done on the impact of supersonic vibrations in conventional devices such as rectangular chambers [18]. Some test results have indicated that, under specific circumstances, the supersonic vibrations can enhance the overall coefficient of heat transfer up to around 300% [16]. Moreover, some other researchers, such as Yao et al. [19] carried out a detailed survey on the augmentation of heat transfer

* Corresponding author at: Ton Duc Thang University, Ho Chi Minh City, Vietnam.
E-mail addresses: mohsen.hashemzadeh@gmail.com (S.. Hashem Zadeh), m.ghodrat@unsw.edu.au (M. Ghodrat), mohammad.ghalambaz@tdtu.edu.vn (M. Ghalambaz).

https://doi.org/10.1016/j.icheatmasstransfer.2021.105345

Available online 11 June 2021

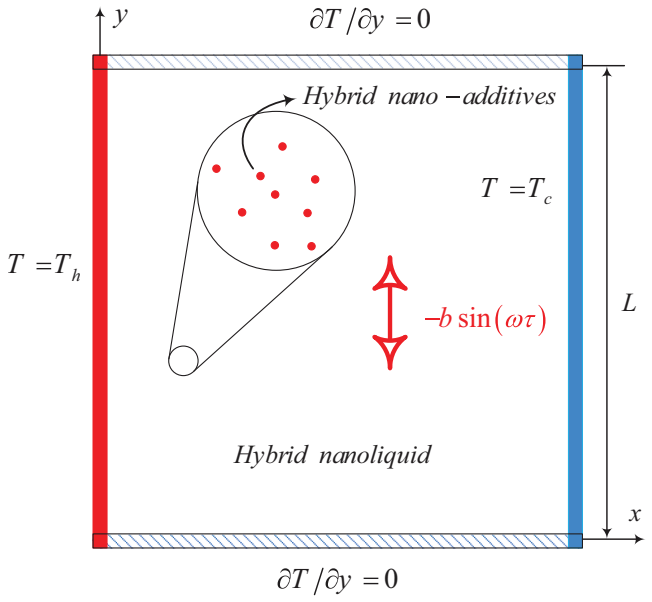

Fig. 1. Computation domain and boundary conditions.

in a shell-and-tube (water-water) supported by power supersonic. They concluded that both ultrasonic power and water flow rate make a considerable impact on the enhancement of heat transfer. Gould et al. [20] ran an experimental and numerical analysis to explore the impact of mechanical vibration on the rate of heat transfer in heat exchangers with viscous dissipation. They showed the rate of heat transfer escalated in a linear make-up with increasing the vibration amplitude. In another study, Shokouhmand and his coauthors [21] analyzed the influence of having flexible vibration on the shell and tube heat exchanger and realized, these vibrations both balance and improve the effect of viscous dissipations on heat transfer coefficient.

Additionally, there are some attempts to determine the impact of nanofluids heat transfer [22]. Liang Zhang et al. [23] analyzed the impact of mechanical vibration on forced convection heat transfer for SiO2–water nanofluids. They realized adding nanoparticles to water or forcing a transverse vibration on the heat transfer surface leads to an increase in heat transfer coefficient. Using both methods simultaneously results in a 182% increase in heat transfer coefficient. However, not much work has been published in the area of integrated vibrations on nanofluids heat transfer enhancement by now.

Hybrid nanoliquid as an expansion of nanoliquid is achieved by diffusing composite nano-powder or two separate nanoparticles in the base fluid. Hybrid nanoliquid can offer acceptable thermal features comparing to their base fluid and even the nanoliquid having single nanoparticles. This is due to their synergistic effects [24]. Hybrid nanofluids demonstrate exceptionally improved thermal properties. Heat transfer characteristics of different hybrid nanoliquid at various operating conditions .have been studied both experimentally and numerically by many researchers.

Jha and Ramaprabhu [25] found hybridizing silver nanoparticles with multi-walled carbon nanotube helps in higher enhancement in thermal conductivity. Some other researchers, such as Ho and his co-authors [26] analyzed the effect of the hybrid Al_2O_3 nanoparticle and microencapsulated phase change material particles on the cooling process's effectiveness and proved that the impact is significant. Suresh et al. [27] realized that Al_2O_3-Cu hybrid results in thermal conductivity enhancement up to 12.11% at a volume fraction of 2%. The hybrid nanofluids were proved to lead to a good enhancement of heat transfer coefficient compared to water; this is found by Balla and his co-authors [28], who numerically investigate the enhancement of heat transfer of CuO-Cu nanofluids flowing with constant heat flux in a circular pipe.

Additionally, Shahsavar et al. [29] explored the forced convection heat transfer of a suspension comprising hybrid nanoparticles of tetramethylammonium hydroxide coated Fe_3O_4 and coated carbon nanotube under a magnetic field.. These researchers studied the hybrid nanofluid in heated tube and showed having an external magnetic field results in accumulation of magnetic nano-additives in the direction of magnetic field. As a result of this, interaction between the flow and aggregates augments and hence, both the thermal conductivity and convection heat transfer coefficient increase. Comparable outcomes were found by Goharkhah [30], Lajvardi [31], and Azizian et al. [32].

In general, thermal conductivity is a decisive factor for increasing heat transfer of the hybrid nanoliquid. In nanofluids both thermal conductivity and the rate of heat transfer alters for number of reasons, such as nanoparticle type, stability, size, type of the base fluid, temperature of the fluid etc. [33–35]. The overall heat transfer through a fluid could be controlled by convection mechanism. The convection heat transfer coefficient greatly changes by the thermal conductivity of the base fluid and the nanoparticles.

Looking at the previous studies in this field indicates that there is a serious lack of information on the impact of vibration on the free convection heat transfer of nanofluids. In the present work, the influence of gravitational and vibrational forces on thermal convection heat transfer of a hybrid nanofluid in a square cavity is examined numerically. We focused on the analysis of several key parameters, including the volume fraction of nanoparticles, frequency of vibration, and vibration and gravitational Rayleigh numbers. The outcomes are presented in terms of isotherms and streamlines, average Nusselt number, and average bulk temperature.

2. Problem definition and formulation

The configuration of the studied geometry in this work is illustrated in Fig. 1. Initially ($t = 0$), the fluid in the enclosure is stagnant and at the temperature of T_c. Moreover, neither buoyancy nor vibrational forces are imposed on the fluid. Later ($t > 0$), simultaneously, the right wall is subjected to temperature differences (T_h), and a vertical vibration is imposed on the enclosure with the displacement of $-b\ \sin\ (\omega t)$ and parallel to the direction of gravity. The vibration velocity amplitude $b\omega$ is not large, and hence, the flow is assumed to be laminar and incompressible. As illustrated in Fig. 1, the top and bottom walls are considered as adiabatic. The enclosure is filled by a hybrid nanoliquid in which the host fluid is water, and the hybrid nano-additive is Ag–MgO.

The equations govern the flow, and thermal field are as follows:

$$\frac{\partial u}{\partial x}+\frac{\partial v}{\partial y}=0 \tag{1}$$

$$\rho_{hnf}\left(\frac{\partial u}{\partial t}+u\frac{\partial u}{\partial x}+v\frac{\partial u}{\partial y}\right)=-\frac{\partial p}{\partial x}+\mu_{hnf}\left(\frac{\partial^2 u}{\partial x^2}+\frac{\partial^2 u}{\partial y^2}\right) \tag{2}$$

$$\rho_{hnf}\left(\frac{\partial v}{\partial t}+u\frac{\partial v}{\partial x}+v\frac{\partial v}{\partial y}\right)=-\frac{\partial p}{\partial y}+\mu_{hnf}\left(\frac{\partial^2 v}{\partial x^2}+\frac{\partial^2 v}{\partial y^2}\right)+\rho_{hnf}g\beta_{hnf}(T_{hnf}-T_c)$$
$$+\rho_{hnf}b\omega^2 sin(\omega t)\beta_{hnf}(T-T_c) \tag{3}$$

$$(\rho C_p)_{hnf}\left(\frac{\partial T}{\partial t}+u\frac{\partial T}{\partial x}+v\frac{\partial T}{\partial y}\right)=k_{hnf}\left(\frac{\partial^2 T}{\partial x^2}+\frac{\partial^2 T}{\partial y^2}\right) \tag{4}$$

The subjected boundary conditions on the solid walls to solve the differential equations are:

Table 1
Dependency of the thermal conductivity and the viscosity of Ag–MgO Hybrid nanoliquid on the volume fraction of nano-additives [37].

φ_{hnp} (%)	k_{hnf}/k_{bf}	μ_{hnf}/μ_{bf}	α_r
0	1	1	1
0.56	1.05376	1.063619	1.0555
1.12	1.08296	1.160534	1.0866
1.5	1.13208	1.300207	1.1371
2	1.1573	1.3815	1.1642

Table 2
The thermophysical characteristics of the nanoparticles and the base fluid [36,38].

Particle	C_p (J/kg. K)	k (W/m. K)	$\alpha \times 10^{-7}$ (m^2/s)	$\beta \times 10^5$ (K^{-1})	ρ (kg/m^3)
MgO	955	45	–	1.05	3650
Ag	235	429	1738.6	1.89	10,500
water	4179	0.613	1.47	21	997.1

$$\begin{aligned} &u(0,y,t)=v(0,y,t)=0,\ \ T(0,\mathrm{y},t)=T_h\\ &u(\mathrm{L},y,t)=v(\mathrm{L},y,t)=0,\ \ T(\mathrm{L},\mathrm{y},t)=T_c\\ &u(x,0,t)=v(x,0,t)=0,\ \ \frac{\partial T(\mathrm{x},0,t)}{\partial y}=0\\ &u(x,\mathrm{L},t)=v(\mathrm{x},\mathrm{L},t)=0,\ \ \frac{\partial T(\mathrm{x},0,t)}{\partial y}=0\\ &u(x,y,0)=0,v(\mathrm{x},y,0)=0,\ \ T(\mathrm{x},y,0)=T_c \end{aligned} \tag{5}$$

These dimensionless parameters are used to convert the dimensional equations to dimensionless those:

$$\begin{aligned} &X=\tfrac{x}{L},\ \ Y=\tfrac{y}{L},\ \ \tau=\tfrac{t\alpha_{bf}}{L^2},\ \ U=\tfrac{uL}{\alpha_{bf}},\ \ V=\tfrac{vL}{\alpha_{bf}},\\ &\theta=\frac{T-T_c}{T_h-T_c},\ \ P=\frac{L^2p}{\rho_{bf}\alpha_{bf}^2},\ \ \Omega=\frac{\omega L^2}{\alpha_{bf}} \end{aligned} \tag{6}$$

Using these non-dimensional parameters, the equations are:

$$\frac{\partial U}{\partial X}+\frac{\partial V}{\partial Y}=0 \tag{7}$$

$$\rho_r\left(\frac{\partial U}{\partial \tau}+U\frac{\partial U}{\partial X}+V\frac{\partial U}{\partial Y}\right)=-\frac{\partial P}{\partial X}+\mu_r Pr\left(\frac{\partial^2 U}{\partial X^2}+\frac{\partial^2 U}{\partial Y^2}\right) \tag{8}$$

$$\begin{aligned} \rho_r\left(\frac{\partial V}{\partial \tau}+U\frac{\partial V}{\partial X}+V\frac{\partial V}{\partial Y}\right)=&-\frac{\partial P}{\partial Y}+\mu_r Pr\left(\frac{\partial^2 V}{\partial X^2}+\frac{\partial^2 V}{\partial Y^2}\right)+Ra_g Pr\rho_r\beta_r\theta\\ &+PrRa_\omega\rho_r\beta_r\theta sin(\Omega\tau) \end{aligned} \tag{9}$$

$$\frac{\partial \theta}{\partial \tau}+U\frac{\partial \theta}{\partial X}+V\frac{\partial \theta}{\partial Y}=\alpha_r\left(\frac{\partial^2 \theta}{\partial X^2}+\frac{\partial^2 \theta}{\partial Y^2}\right) \tag{10}$$

where Ra_g, Ra_w, and Pr are gravitational Rayleigh, vibration Rayleigh, and Prandtl numbers:

$$Ra_g=\frac{g\beta_{bf}\Delta TL^3}{\nu_{bf}\alpha_{bf}},Ra_\omega=\frac{b\omega^2\beta_{bf}\Delta TL^3}{\nu_{bf}\alpha_{bf}},Pr=\frac{\upsilon_{bf}}{\alpha_{bf}} \tag{11}$$

Additionally, the mentioned ratios are:

$$\rho_r=\frac{\rho_{hnf}}{\rho_{bf}},\ \ \mu_r=\frac{\mu_{hnf}}{\mu_{bf}},\ \ \beta_r=\frac{\beta_{hnf}}{\beta_{bf}},\ \ \alpha_r=\frac{\alpha_{hnf}}{\alpha_{bf}},\ \ \alpha_{hnf}=\frac{k_{hnf}}{(\rho C_p)_{hnf}} \tag{12}$$

Furthermore, the dimensionless forms of boundary conditions can be written as follows:

$$\begin{aligned} &U(0,Y,\tau)=V(0,Y,\tau)=0,\theta(0,\mathrm{Y},\tau)=1\\ &U(1,Y,\tau)=V(1,\mathrm{Y},\tau)=0,\theta(1,\mathrm{Y},\tau)=0\\ &U(\mathrm{X},0,\tau)=V(X,0,\tau)=0,\frac{\partial\theta(\mathrm{X},0,\tau)}{\partial Y}=0\\ &U(X,1,\tau)=V(X,1,\tau)=0,\frac{\partial\theta(\mathrm{X},0,\tau)}{\partial Y}=0\\ &U(X,Y,0)=0,V(X,Y,0)=0,\ \ T(X,Y,0)=0 \end{aligned} \tag{13}$$

A perfect review of the hybrid nanoliquid shows that there is no certain relation to calculate the values of thermo-physical properties of these types of suspensions. Hence, the current study employs the experimental data of the Ag–MgO Hybrid nanoliquid properties, as depicted in Table 1. Also, the remaining thermophysical properties could be obtained from Eqs. (14)–(17) [36].

$$(\rho c_p)_{hnf}=(1-\varphi_{hnp})(\rho c_p)_{bf}+\varphi_{MgO}(\rho c_p)_{MgO}+\varphi_{Ag}(\rho c_p)_{Ag} \tag{14}$$

$$(\rho\beta)_{hnf}=(1-\varphi_{hnp})(\rho\beta)_{bf}+\varphi_{MgO}(\rho\beta)_{MgO}+\varphi_{Ag}(\rho\beta)_{Ag} \tag{15}$$

$$\rho_{hnf}=\rho_f(1-\varphi_{hnp})+\rho_{MgO}\varphi_{MgO}+\rho_{Ag}\varphi_{Ag} \tag{16}$$

$$\alpha_{hnf}=k_{hnf}\Big/(\rho c_p)_{hnf} \tag{17}$$

Further, the thermophysical characteristics of the components of the hybrid nano-additives are tabulated in Table 2.

The local Nusselt number on the hot wall can be achieved as

$$Nu_{local}=-\frac{k_{hnf}}{k_{bf}}\left(\frac{\partial\theta}{\partial X}\right) \tag{18}$$

By integrating the local Nusselt number over the left hot wall, the average Nusselt number can be reached as

$$Nu_{avg}=-\frac{k_{hnf}}{k_{bf}}\int_0^1\left(\frac{\partial\theta}{\partial X}\right)dY \tag{19}$$

The bulk average temperature, θ_a, is defined as the following:

$$\theta_a=\int_0^1\int_0^1\theta dXdY \tag{20}$$

3. The procedure of solution, grid independence, and validation

The Galerkin finite element method is employed to solve the discussed set of non-linear, coupled, and non-dimensional governing equations. The numerical method has been completely detailed in [39,40]. In this method, a penalty parameter is employed to replace the pressure gradient terms in the momentum equations. The penalty parameter can be defined as [39]:

$$P=-\gamma\left(\frac{\partial U}{\partial X}+\frac{\partial V}{\partial Y}\right) \tag{21}$$

The point about the penalty parameter is that for high values of γ, the mass conservation equation will be satisfied automatically. Substituting Eq. (19) in Eqs. (8) and (9) results in the following form of the momentum equations:

$$\rho_r\left(\frac{\partial U}{\partial \tau}+U\frac{\partial U}{\partial X}+V\frac{\partial U}{\partial Y}\right)=\gamma\frac{\partial}{\partial X}\left(\frac{\partial U}{\partial X}+\frac{\partial V}{\partial Y}\right)+\mu_r Pr\left(\frac{\partial^2 U}{\partial X^2}+\frac{\partial^2 U}{\partial Y^2}\right) \tag{22}$$

$$\begin{aligned} \rho_r\left(\frac{\partial V}{\partial \tau}+U\frac{\partial V}{\partial X}+V\frac{\partial V}{\partial Y}\right)=&\gamma\frac{\partial}{\partial Y}\left(\frac{\partial U}{\partial X}+\frac{\partial V}{\partial Y}\right)+\mu_r Pr\left(\frac{\partial^2 V}{\partial X^2}+\frac{\partial^2 V}{\partial Y^2}\right)\\ &+Ra_g Pr\rho_r\beta_r\theta+PrRa_\omega\rho_r\beta_r\theta sin(\Omega\tau) \end{aligned} \tag{23}$$

In the finite element method, the equations are first converted to a

weak form and then expanded using basic functions. In the present study, a linear basis function ($\xi_k|_{k=1}^{M}$) is used to expand all the variables (U, V, θ) in the computational domain:

$$U \approx \sum_{k=1}^{M} U_k \xi_k(X,Y), V \approx \sum_{k=1}^{M} V_k \xi_k(X,Y), \theta \approx \sum_{k=1}^{M} \theta_k \xi_k(X,Y) \tag{24}$$

With the above expansions and applying the Galerkin finite element method, the residual equations for the internal nodes will be obtained as:

$$R_i^1 = \rho_r \sum_{k=1}^{M} U_k \int_\Omega \frac{\partial \xi_k}{\partial \tau} \xi_i dXdY + \rho_r \sum_{k=1}^{M} U_k \int_\Omega \left[\left(\sum_{k=1}^{M} U_k \xi_k \right) \frac{\partial \xi_k}{\partial X} + \left(\sum_{k=1}^{M} V_k \xi_k \right) \frac{\partial \xi_k}{\partial Y} \right] \xi_i dXdY +$$
$$\gamma \sum_{k=1}^{M} U_k \int_\Omega \frac{\partial \xi_i}{\partial X} \frac{\partial \xi_k}{\partial X} dXdY + \gamma \sum_{k=1}^{M} V_k \int_\Omega \frac{\partial \xi_i}{\partial X} \frac{\partial \xi_k}{\partial Y} dXdY + \tag{25}$$
$$\mu_r Pr \sum_{k=1}^{M} U_k \int_\Omega \left[\frac{\partial \xi_i}{\partial X} \frac{\partial \xi_k}{\partial X} + \frac{\partial \xi_i}{\partial Y} \frac{\partial \xi_k}{\partial Y} \right] dXdY$$

$$R_i^2 = \rho_r \sum_{k=1}^{M} U_k \int_\Omega \frac{\partial \xi_k}{\partial \tau} \xi_i dXdY + \rho_r \sum_{k=1}^{M} V_k \int_\Omega \left[\left(\sum_{k=1}^{M} U_k \xi_k \right) \frac{\partial \xi_k}{\partial X} + \left(\sum_{k=1}^{M} V_k \zeta_k \right) \frac{\partial \xi_k}{\partial Y} \right] \xi_i dXdY +$$
$$\gamma \sum_{k=1}^{M} U_k \int_\Omega \frac{\partial \xi_i}{\partial Y} \frac{\partial \xi_k}{\partial X} dXdY + \gamma \sum_{k=1}^{M} V_k \int_\Omega \frac{\partial \xi_i}{\partial Y} \frac{\partial \xi_k}{\partial Y} dXdY + \tag{26}$$
$$\mu_r Pr \sum_{k=1}^{M} V_k \int_\Omega \left[\frac{\partial \xi_i}{\partial X} \frac{\partial \xi_k}{\partial X} + \frac{\partial \xi_i}{\partial Y} \frac{\partial \xi_k}{\partial Y} \right] dXdY +$$
$$Ra_g Pr \rho_r \beta_r \int_\Omega \sum_{k=1}^{M} \theta_k \xi_k(X,Y) + PrRa_\omega \rho_r \beta_r \int_\Omega \sum_{k=1}^{M} \theta_k sin(\Omega\tau) \xi_k(X,Y)$$

$$R_i^3 = \sum_{k=1}^{M} \theta_k \int_\Omega \frac{\partial \xi_k}{\partial \tau} \xi_i dXdY + \sum_{k=1}^{M} \theta_k \int_\Omega \left[\left(\sum_{k=1}^{M} U_k \xi_k \right) \frac{\partial \xi_k}{\partial X} + \left(\sum_{k=1}^{M} V_k \xi_k \right) \frac{\partial \xi_k}{\partial Y} \right] \xi_i dXdY$$
$$+ \alpha_r \sum_{k=1}^{M} \theta_k \int_\Omega \left[\frac{\partial \xi_i}{\partial X} \frac{\partial \xi_k}{\partial X} + \frac{\partial \xi_i}{\partial Y} \frac{\partial \xi_k}{\partial Y} \right] dXdY \tag{27}$$

The second-order Gaussian-quadrature method is utilized for integrating the residual equations. Further, for accurate capture of the effect of vibration on the flow and thermal fields, a variable time step, based on the frequency of oscillation is employed [41]:

$$\Delta\tau^{n+1} = \begin{cases} 10^{-5} & \tau \le 0.02 \\ min\left(1.02\Delta\tau^n, \frac{1}{128}\frac{2\pi}{\Omega}\right) & \tau \ge 0.02 \end{cases} \tag{28}$$

where n is the iteration number. Moreover, the following stopping criterion is considered for the process:

$$\sqrt{\left(R_i^1\right)^2 + \left(R_i^2\right)^2 + \left(R_i^3\right)^2} \le 10^{-6} \tag{29}$$

As shown in Fig. 2, for the case of high non-dimensional frequency ($\Omega = 5000$), the values of the average Nusselt numbers obtained by six grids with different resolutions have been used for the grid check. A non-uniform structured grid with an element growth ratio of 5.0 has been utilized to ensure that the high velocity and temperature gradients are precisely captured at the solid walls. Details of the studied grids and the computational times are shown in Table 3. Owing to the imposed vibrational force, the average Nusselt number oscillates with the frequency of the cavity displacement. It can be seen that the results of case No. 4 with 10,000 (100×100) elements have a feeble discrepancy with the finer grids of 125×125 and 150×150 elements and could be employed for the simulations in the present study.

The finite element code has been validated against three different research to ensure the outcomes are appropriately and accurately calculated. First, the results of the developed finite element code are compared with the experimented outcomes of Corvaro and Paroncini [42] and shown in Fig. 3. In [42], the natural convection heat transfer of air ($Pr = 0.71$) in a 0.05 m square enclosure with a rectangular heater has been surveyed experimentally. Further, a 2-D-PIV system was implemented for visualizing the flow field. In experiments of Corvaro and Paroncini [42], the cold walls were isothermally kept at 291.16 K, and the temperature of the hot walls was changed to provide different Rayleigh numbers. As seen, the isolevels of velocity magnitude are in close agreement with those obtained by 2-D-PIV system experimentations, specifying that the flow and thermal fields are accurately modeled and solved.

For the second case, outcomes presented by Fu et al. [41] have been employed for comparison. In [41], transient mixed convection of air ($Pr = 0.71$) in a square cavity is analyzed under the simultaneous effect of gravity and vibration. The side walls in the paper of Fu et al. [41] are heated isothermally, and the top and bottom walls are considered to be adiabatic. The air in the cavity is stationary and in thermal equilibrium with the cold wall. Simultaneously, a temperature rise is applied to the left wall, and the vibration is imposed on the cavity for $\tau \ge 0$. A tight comparison has been performed to guarantee that the vibration effects have

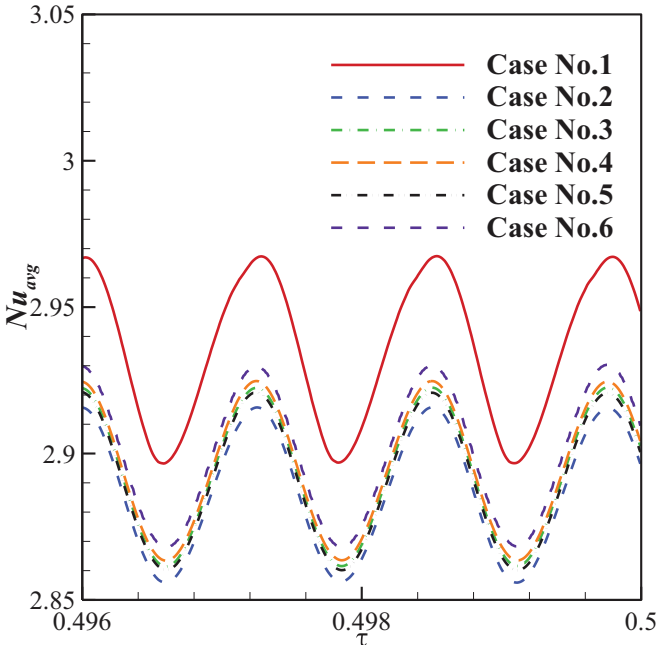

Fig. 2. The variations of the Nusselt number on right boundary versus the dimensionless time in different mesh at $\Omega = 5000$, $\varphi_{hnp} = 2$, $Ra_g = 10^5$, $Ra_\omega = 10^6$.

Table 3
Run time of differnce mesh at $\Omega = 5000$, $\varphi_{hnp} = 2$, $Ra_g = 10^5$, $Ra_\omega = 10^6$.

Case no.	1	2	3	4	5	6
No. of Elements	25 × 25	50 × 50	75 × 75	100 × 100	125 × 125	150 × 150
Time (min)	186	321	622	1179	1292	1486

been accurately modeled and calculated. Owing to the considered initial condition, the heat transfer rate on the side walls is different at the early stages of the simulations. Fig. 4 shows the values of averaged Nusselt numbers on the right and left boundaries for a high value of non-dimensional frequency ($\Omega = 5000$) for the present study and those presented by Fu et al. [41]. As seen, the values of Nu_{avg} are in close agreement

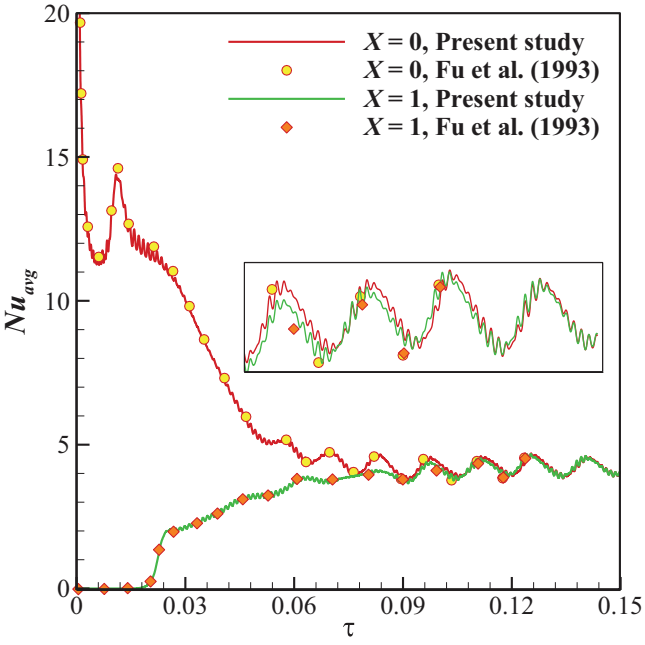

Fig. 4. Time variation of the average numbers on the right ($X = 1$) and left ($X = 0$) boundaries ($Ra_g = 10^4$, $Ra_\omega = 7.07 \times 10^6$, $\Omega = 5000$): comparison between the present study and Fu et al. [41].

with [41]. Further, the obtained flow and thermal fields at $\tau = 5.4978 \times 10^{-3}$ are compared with those presented by Fu et al. [41] In Fig. 5. Besides, the average values of the Nusselt number and the maximum and minimum values of streamlines are presented in Table 4. It should be noted that the plus (+) and cross (×) signs in the streamlines indicate the place of maximum (clockwise) and minimum (counter-clockwise) vortexes in the cavity. As seen, an admissible agreement can be found, representing that the developed finite element code can precisely simulate the flow and heat transfer in the cavity under the vibrational and gravitational effects.

As the final stage, the present study work has been compared with the research done by Kahveci [43] and shown in Fig. 6. Kahveci [43] numerically studied the thermo-gravitational flow of various nanofluids inside a tilted square cavity. The boundary conditions are the same as the

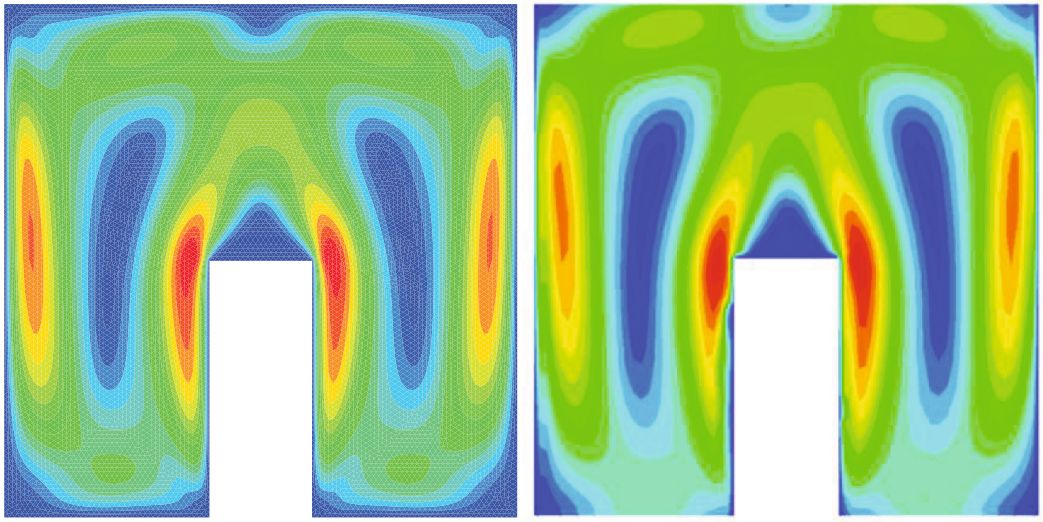

Fig. 3. The isolines of velocity magnitude of air in a cavity with a rectangular heater ($Ra_g = 3.16 \times 10^5$, $d = 0.4$, $Pr = 0.71$): Comparison between the present study (left) and the experimentations of Corvaro and Paroncini [42] (right).

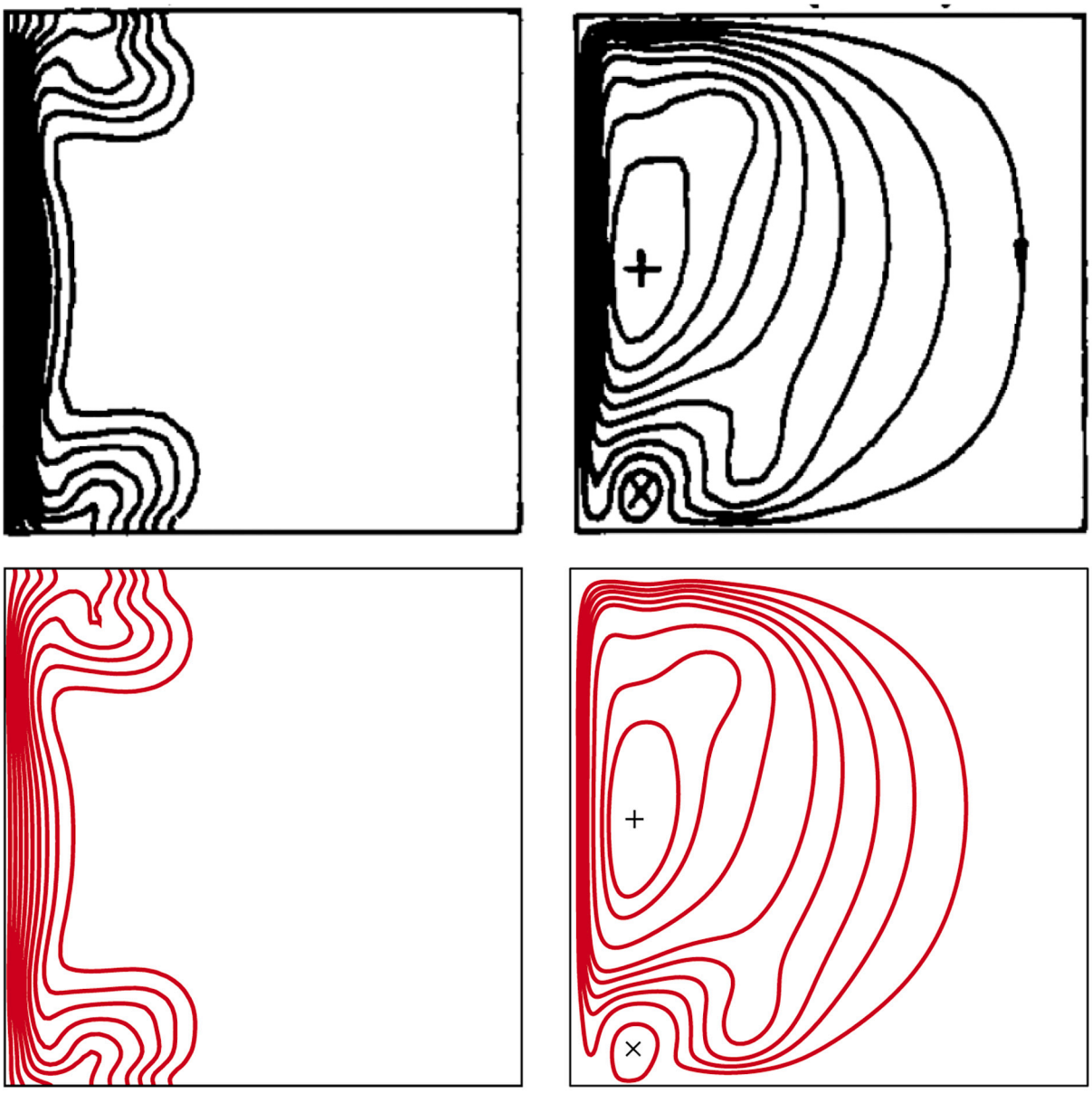

Fig. 5. The streamlines and isotherms of air in a cavity under vibration ($Ra_g = 10^4$, $Ra_\omega = 7.07 \times 10^6$, $\Omega = 5000$ and $\tau = 5.4978 \times 10^{-3}$): comparison between the outcomes of the present work and Fu et al. [41].

present study, and the problem is solved for the steady-state condition. Five different water-based nanofluids comprising Cu, Ag, CuO, Al_2O_3, and TiO_2 are studied, and the inclination angle is varied from 0° to 90°. An excellent agreement is evident between the present result and those calculated by Kahveci [43] for two values of the gravitational Rayleigh number ($Ra_g = 10^5$ and 10^6). With the above grid check and comparisons, the accuracy and correctness of the results are assured and outcomes are both independent to the gird and exact.

Table 4
Values of the average Nusselt number on the right ($X = 1$) and the left ($X = 0$) boundaries and extremum values of the streamfuction ($Ra_g = 10^4$, $Ra_\omega = 7.07 \times 10^6$, $\Omega = 5000$ and $\tau = 5.4978 \times 10^{-3}$): comparison between the present study and Fu et al. [41].

	Nu_{avg} $(X = 1)$	Nu_{avg} $(X = 0)$	Ψ_{min}	Ψ_{max}
Fu et al. [41]	0.0	11.4	−31.0	4.68
Present study	0.0	11.28	−30.65	4.44

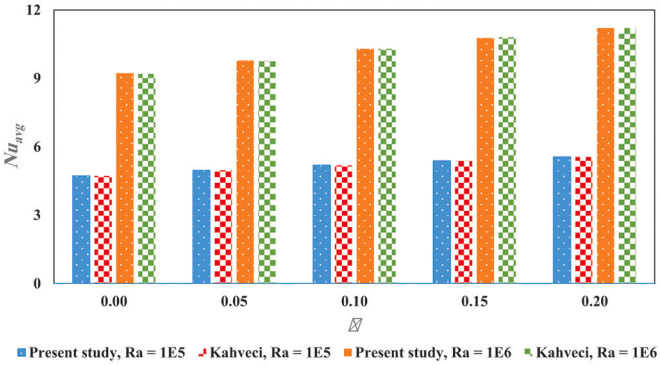

Fig. 6. Effect of volume fraction of Al_2O_3 nanoparticles on the average Nusselt number ($Pr = 6.2$, $\beta = 0.02$, $\theta = 0°$, $Ra_\omega = \Omega = 0$): comparison between the outcomes of Kahveci [44] and the present study.

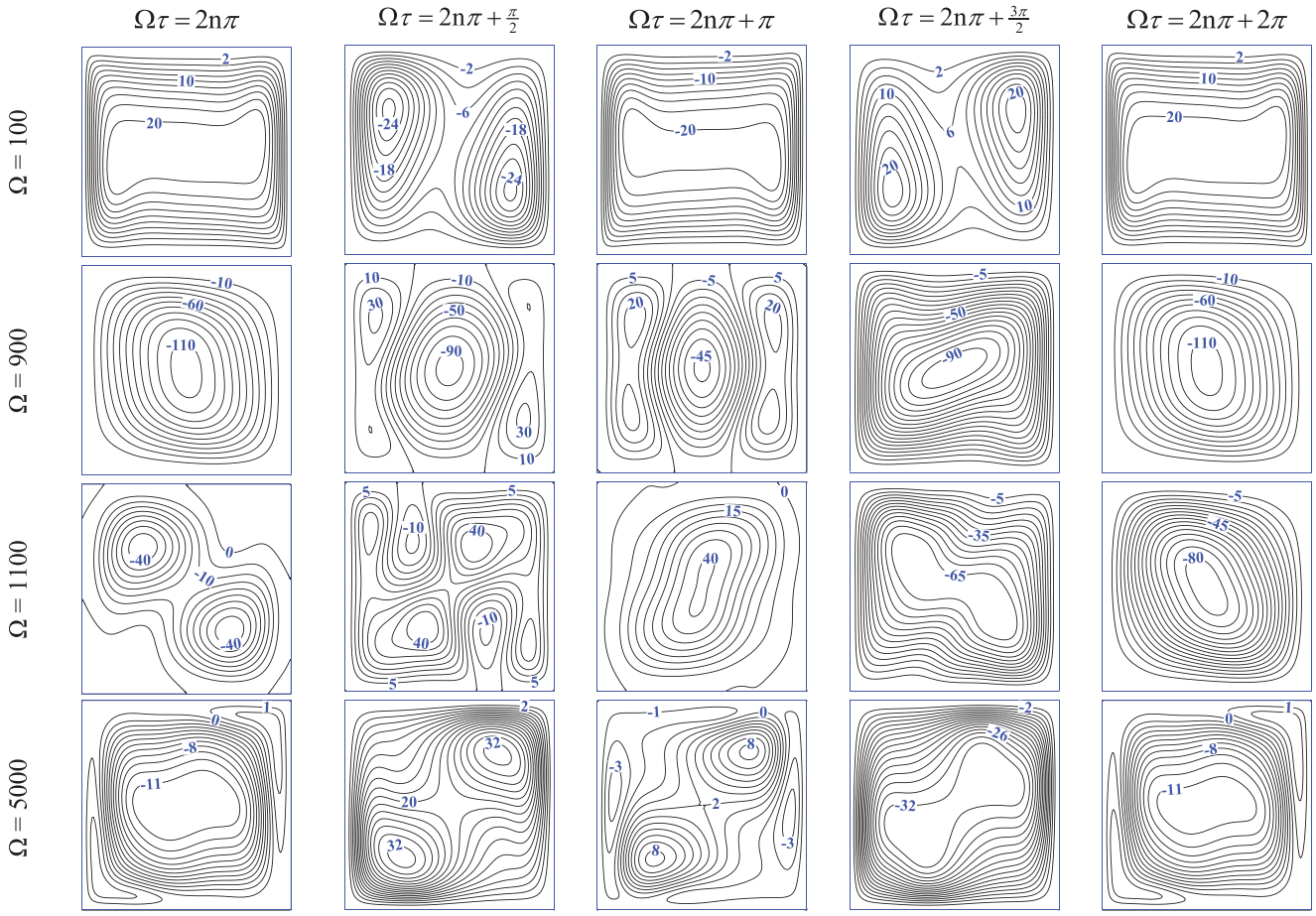

Fig. 7. Hybrid nanofluid streamlines in a complete period of oscillation in the quasi-steady state ($\varphi_{hnp} = 1.12$, $Ra_g = 10^4$, $Ra_\omega = 10^6$).

4. Results and discussion

Figs. 7 and 8 illustrate, respectively, the streamlines and the isotherms of the nanofluid during a period of oscillation in the quasi-steady state. The flow in the cavity is induced by two factors: a mechanical one due to the vibration of the cavity and a thermal one due to the free convection due to the difference in temperature between the side walls, where the hot and cold zones of the fluid motion, respectively, upwards and downwards leading to a clockwise circulation. In the first half-period ($\Omega\tau$ between $2n\pi$ and $2n\pi + \pi$), the cavity goes down, weakening the buoyancy forces, while these forces are intensified in the second half-period ($\Omega\tau$ between $2n\pi + \pi$ and $2n\pi + 2\pi$) when the motion of the cavity is upwards. For $\Omega = 100$, the cavity starts with one recirculation zone in the counter-clock wise direction. The recirculation zone then splits into two zones in the opposite flow direction when the cavity goes down to its lowest ($\Omega\tau = 2n\pi + \pi/2$). Once the cavity goes back to the initial position ($\Omega\tau = 2n\pi + \pi$), the flow goes back to a one recirculation zone, but in the clockwise direction. When the cavity goes up, the same trend appears, but with inverse directions: first, two zones appear in the counter-clockwise direction and then go back to one recirculation zone after one complete period. In this case, the isotherms are concentrated vertical lines near the side walls and horizontal lines in the core. The horizontal lines become inclined, following the flow patterns and the direction of the recirculation zones, when the cavity is going up or down in its vibratory motion. For $\Omega = 9000$, the flow starts with a clockwise recirculation zone. Once the cavity goes down, the change of the buoyancy effects in the flow leads to the creation of two vortices near the side walls, surrounding the recirculation zone present in the core of the cavity. As the cavity goes up, the flow regains its initial pattern progressively after one complete period. The isotherms are more distributed throughout the cavity compared to the first case and are more unstructured during the cavity vibration. In the case $\Omega = 1100$, the flow patterns are considerably disturbed by the vibration, as several vortices appear when the cavity is descending. More interestingly, the streamlines are not the same after one complete period, indicating that the quasi-steady state is not reached in this case. Following the streamlines, the temperature distribution shows an important disturbance, indicating the intensity of mixing between the cold and hot regions of the flow. The change in the isotherms distribution after one complete period of vibration is also observed. This irregularity in the flow and isothermal patterns can be attributed to resonant effects, i.e., when the period of the external vibration is close to the resonance period of the flow. For $\Omega = 5000$, the flow shows the same patterns after one complete period compared to the initial patterns, so the quasi-steady state is attained. Despite the change in the isotherms during the vibration, the isotherms show almost the same pattern with time. This can be attributed to the very short period of vibration. The fluid cannot catch up with the variations due to the vibration, keeping thus the same temperature distribution. All these observations indicate that the vibration leads to time-dependent flow and isotherm patterns and that the direction of flow circulation is not always similar, at the same considered instant, when Ω is

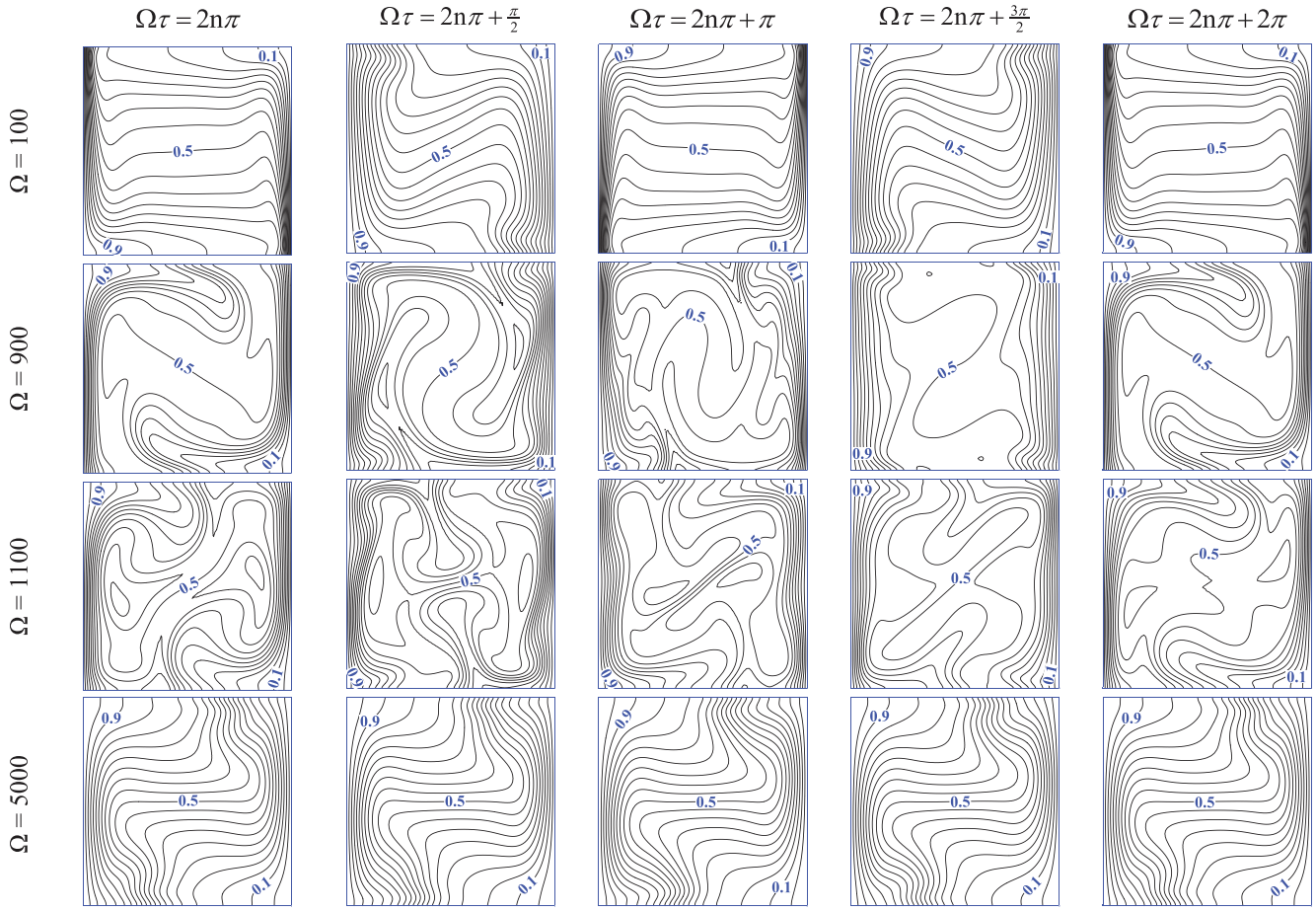

Fig. 8. Hybrid nanofluid streamlines in a complete period of oscillation in the quasi-steady state ($\varphi_{hnp} = 1.12$, $Ra_g = 10^4$, $Ra_\omega = 10^6$).

varied. Consequently, the intensity of heat transfer fluctuates, according to Ω. The impact of Ω and other various parameters on the characteristics of heat transfer in the enclosure is analyzed in the following.

Fig. 9 shows the variation of the Nu_{avg} on the right boundary as a function of time for different values of the angular frequency Ω. It can be seen that the value of Nu_{avg} follows a periodic fluctuation with a period

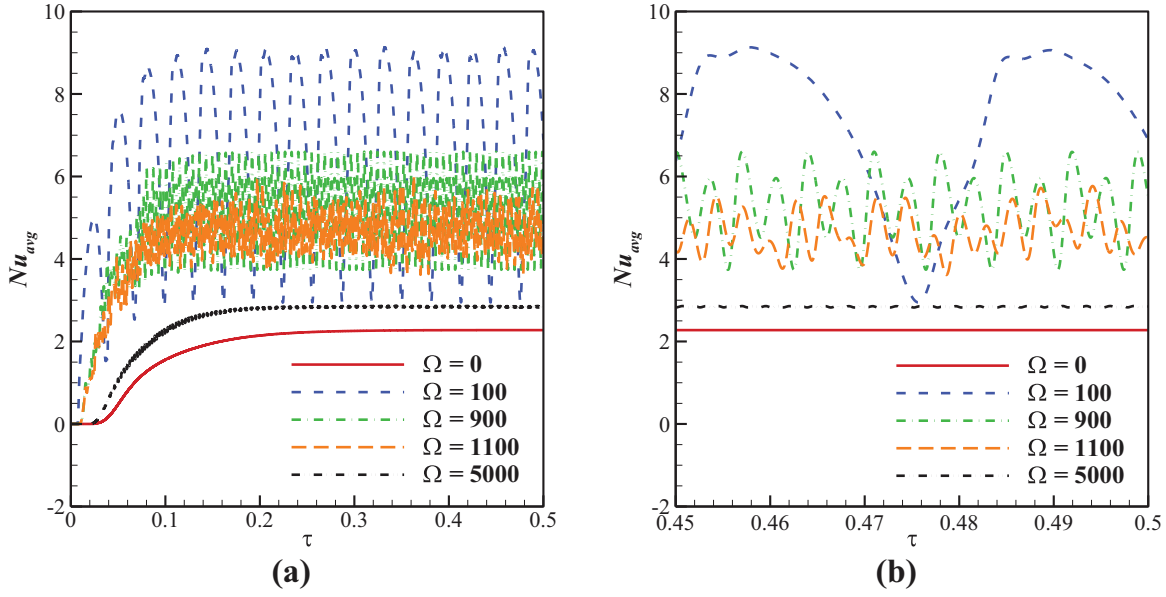

Fig. 9. Variations of the average Nusselt number on the right boundary versus the dimensionless time for different values of the Ω ($\varphi_{hnp} = 1.12$ at $Ra_g = 10^4$, $Ra_\omega = 10^6$): (a) for all of the dimensionless time. (b) a closer look on $0.45 \leq \tau \leq 0.50$.

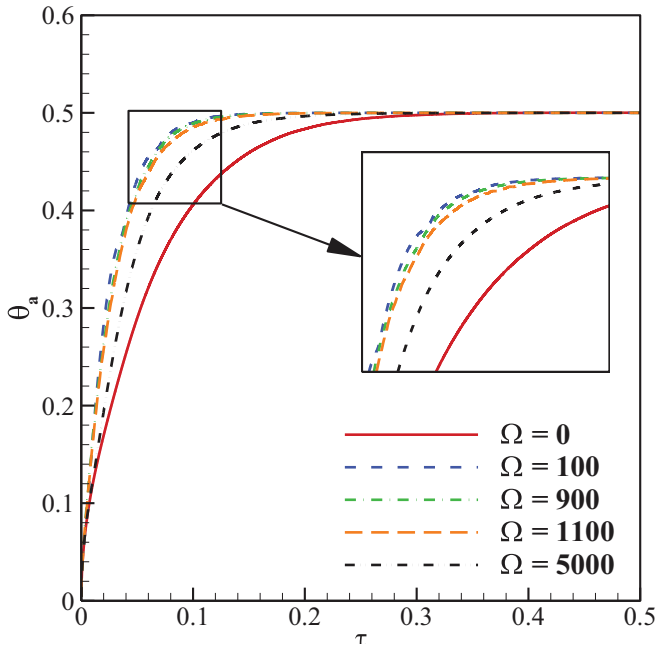

Fig. 10. The variations of the average bulk temperature versus the dimensionless time for different values of Ω ($\varphi_{hnp} = 1.12$ at $Ra_g = 10^4$, $Ra_\omega = 10^6$).

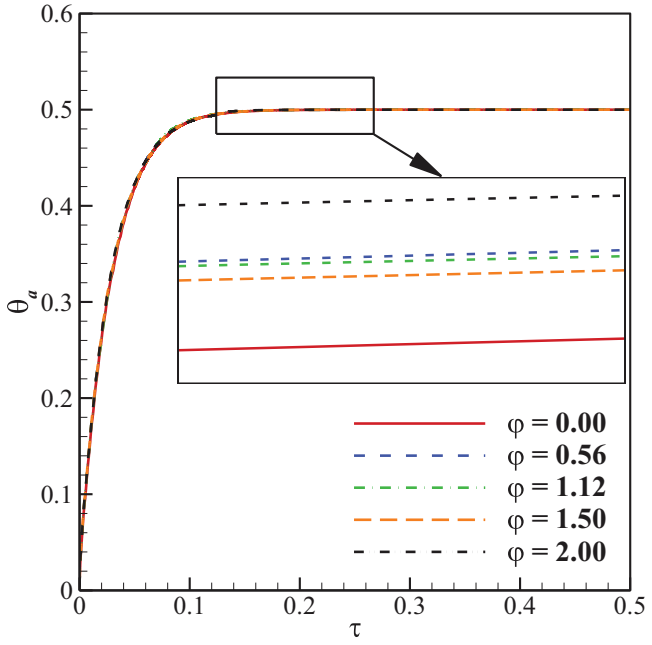

Fig. 12. The variations of the bulk average temperature versus the dimensionless time for different values of φ_{hnp} (Ω = 900, $Ra_g = 10^4$, $Ra_\omega = 10^6$).

inversely proportional to Ω, except for the two cases Ω = 0 and Ω = 5000. The first case corresponds to a non-vibrating cavity, and in the second one, the period of the cavity vibration is shorter than the time-scale of the thermal boundary layer, thus diminishing the oscillation of Nu_{avg}. For the other cases, the amplitude of Nu_{avg} rises with the decrease of Ω, and it reaches its maximum for Ω = 100. Nu_{avg} is greater, for all the values of Ω≠0, than the case Ω=0, indicating that the heat transfer is enhanced when the cavity is vibrating compared to a static cavity. For Ω = 5000, the value of Nu_{avg} is the closest to a static cavity, as the period of vibration is too small so that the time between intensifying and diminishing the buoyancy forces due to vibration is too short for the flow to be influenced.

The variation of the average bulk temperature θ_a as a function of time is plotted in Fig. 10 as a function of time for various values of Ω. The variation of θ_a is related to that of Nu_{avg}. In fact, the time required for θ_a to reach 0.5 indicates the effectiveness of heating in the cavity. This effectiveness increases for lower values of Ω, while being always greater than the case of a static cavity. This points out the impact of the cavity vibration on heat transfer by inducing changes in the direction of buoyancy effects. This observation can be confirmed by the fact that the case Ω = 5000 has

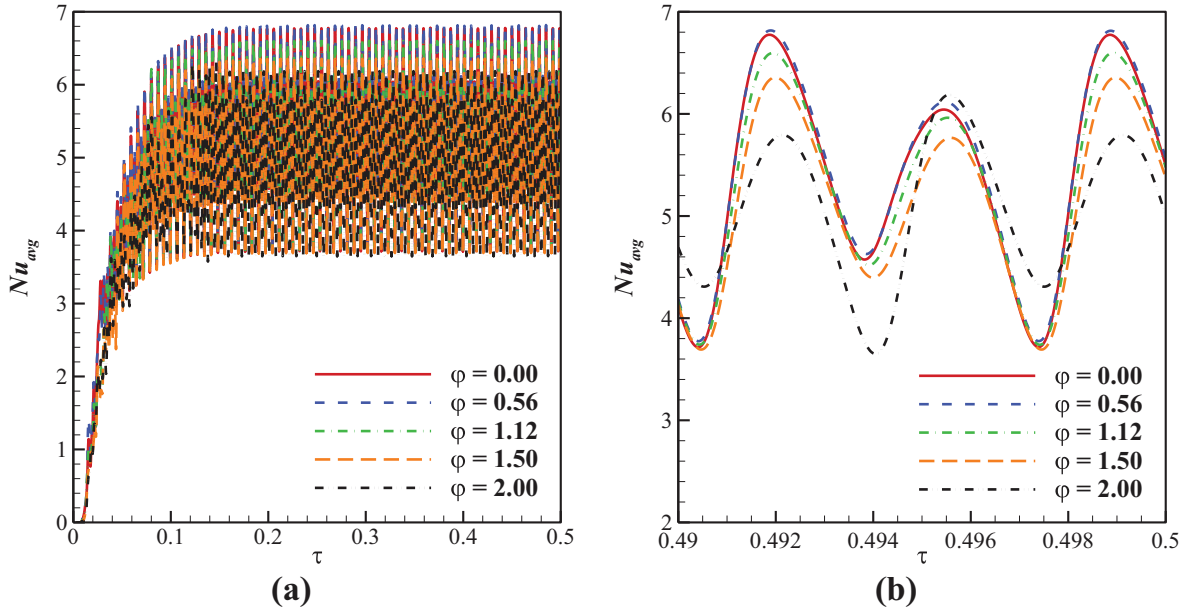

Fig. 11. The variations of the Nusselt number on the right boundary versus the dimensionless time for different values of φ_{hnp} (Ω = 900, $Ra_g = 10^4$, $Ra_\omega = 10^6$) (a) for all of the dimensionless time. (b) a closer look on $0.49 \leq \tau \leq 0.50$.

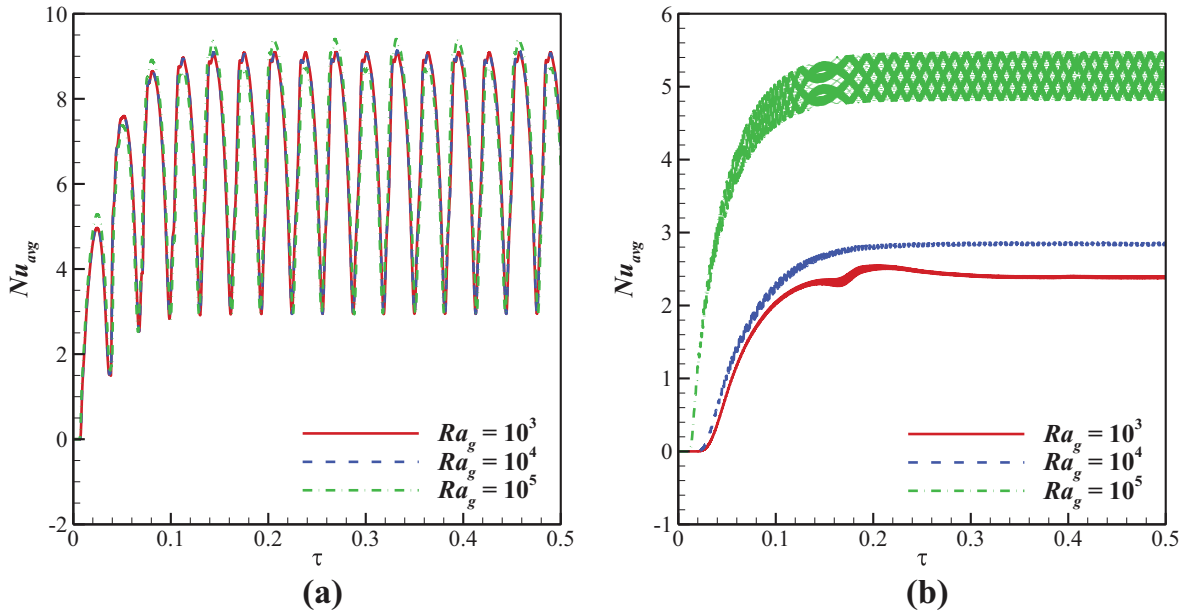

Fig. 13. Impact of gravitational Rayleigh number on the time variation of the average Nusselt number ($\varphi_{hnp} = 1.12$, $Ra_\omega = 10^6$): (a) Ω = 100 (b) Ω = 5000.

the lowest heating effectiveness among the vibrating cavities, as in that case, the vibration effects are minimized due to the very short period, as discussed in Fig. 9.

Fig. 11 depicts the variation of Nu_{avg} as a function of time for different values of the nanoparticle volume fraction φ. The fluctuation of Nu_{avg} shows that the effect of φ varies according to time and depends on which the cavity is ascending or descending during its vibration. ($\tau = 0.492 = 2n\pi + \pi$, with $n = 70$). In fact, the nanoparticles lead to an enhancement of the thermal conductivity, but also to an increase in its thermal conductivity. When the cavity vibratory motion is ascending, the buoyancy forces are intensified, and the viscous resistive effects are diminished so that the negative impact of the nanoparticles on the flow resistance becomes insignificant. In that case, increasing φ tends to raise the value of Nu_{avg}. On the other hand, when the cavity is descending, the buoyancy forces are hindered and the viscous effects become important, so that the impact of the nanoparticles on the viscosity is important. In that case, Nu_{avg} decreases for higher values of φ.

The effect of φ on the variation of θ_a is illustrated in Fig. 12. It is obvious that φ has a slight effect on θ_a. A slight rise in θ_a can be observed with the increase of φ. This shows that while the nanoparticle concentration affects the fluctuations of Nu_{avg}, it has a very limited effect on heating effectiveness.

The variation of Nu_{avg} for various gravitational Rayleigh numbers Ra_g is shown in Fig. 13. It can be seen that Nu_{avg} increases with Ra_g for the two values of Ω shown, and is maximum for $Ra_g = 10^6$. This is related to the definition of Ra_g, which indicates the relative dominance of the buoyancy forces driving the convective flow over viscous forces resisting it. Raising the value of Ra_g, therefore, intensifies the flow and enhances heat transfer.

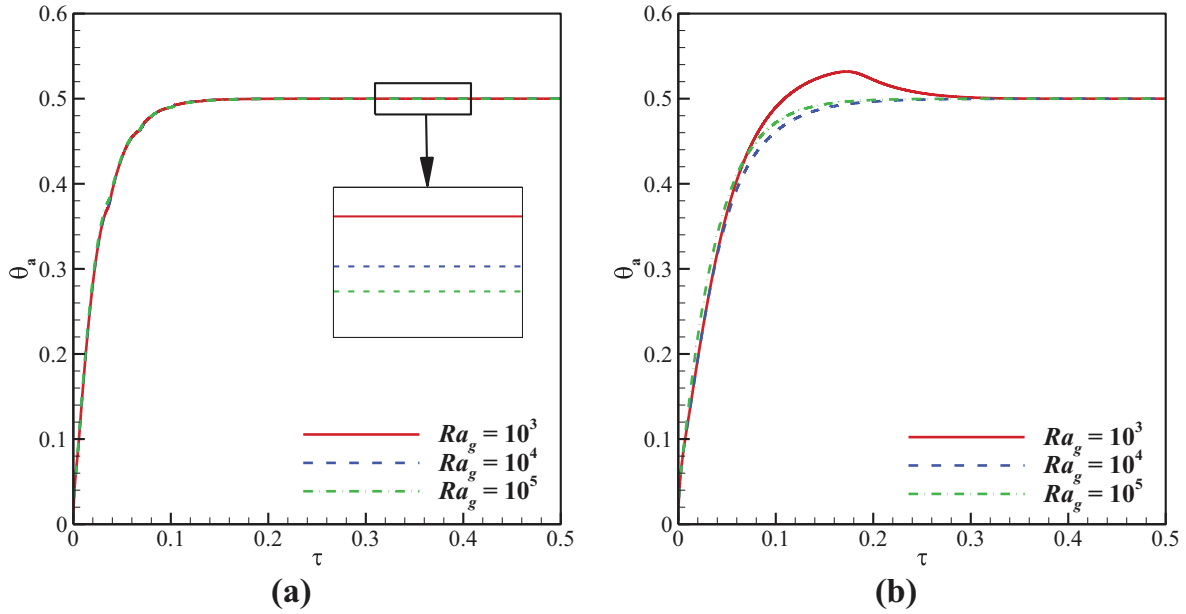

Fig. 14. Impact of gravitational Rayleigh number on the time variation of the bulk temperature ($\varphi_{hnp} = 1.12$, $Ra_\omega = 10^6$): (a) Ω = 100 (b) Ω = 5000.

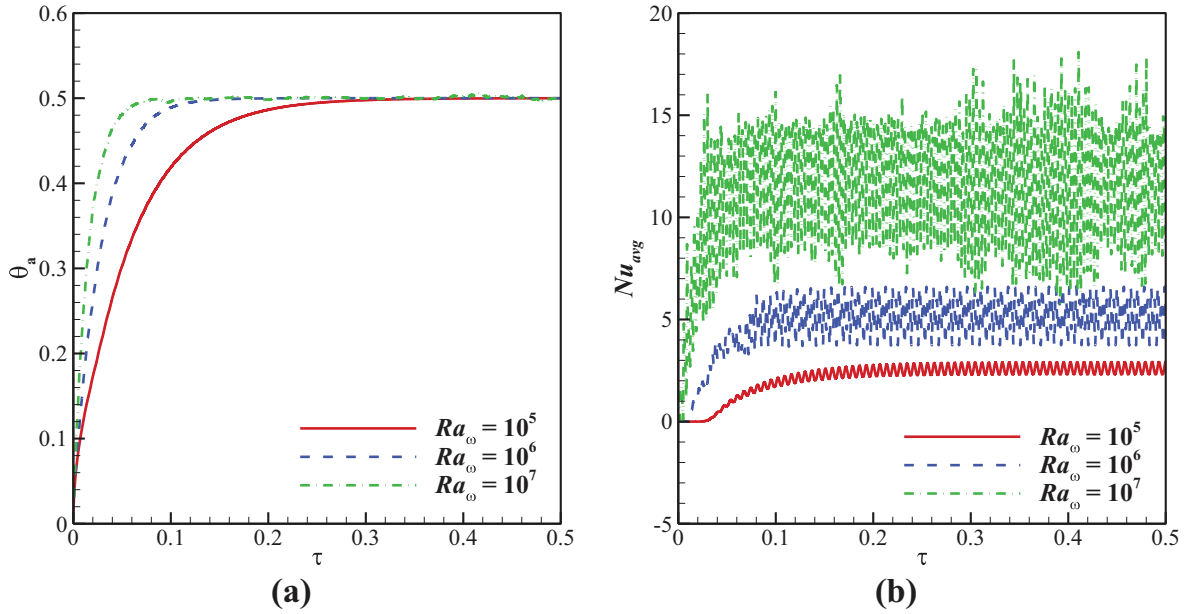

Fig. 15. The variations of (a) the bulk temperature and (b) the average Nusselt versus the dimensionless time for the different values of vibration Rayleigh number ($\varphi_{hnp} = 1.12$, $\Omega = 900$, $Ra_g = 10^4$).

Fig. 14 depicts the time variation of θ_a for three values of Ra_g. It is clear that heating effectiveness is not influenced by Ra_g for $\Omega = 900$. On the other hand, it decreases with Ra_g in the case $\Omega = 5000$ and shows a minimum for $Ra_g = 10^3$. Indeed, when $\Omega = 5000$, the behavior of the cavity is similar to a static one, as the period of vibration is too short for the flow to be affected by the vibration-induced buoyancy fluctuations, and in that case, the relative importance of the free convection effects increases. For lower frequency, the vibration effects are more important so that they damp the intensity of the natural convection so that a similar result is obtained for all the values of Ra_g. This result indicates that the effect of the free convection intensity is more apparent for higher vibration frequencies.

The impact of vibration Rayleigh number Ra_ω on the variations of Nu_{avg} and θ_a as functions of time is presented in Fig. 15. It is clear that increasing Ra_ω raises Nu_{avg} and heating effectiveness. This is due to the augmentation of buoyancy forces due to the cavity vibration, leading to flow intensification and heat transfer improvement. Moreover, it is shown that raising Ra_ω increases the values of Nu_{avg} over time and its fluctuation, which confirms the contribution of the vibration intensity, represented by its amplitude and frequency, to the heat transfer improvement. The results of Figs. 13 and 15 show that, overall, both the free convection and the vibration play a role in heat transfer enhancement in the enclosure.

5. Conclusion

The outcomes of the present investigation can be summed up as follows:

- The flow patterns and temperature distribution in the cavity are altered in the presence of external vibrations, which affects the buoyancy forces in the fluid due to the ascending-descending motion of the cavity. This leads to fluctuations in the intensity of heat transfer and its effectiveness. These fluctuations mainly depend on the frequency of the vibrations and their amplitude. Anyway, the external vibration enhances heat transfer for all the considered frequencies. The effectiveness of heating is also improved in the presence of vibrations.
- The presence of the nanoparticles seems to have a very limited effect on the effectiveness of heating. Nonetheless, the impact of the nano-additive volume fraction on the intensity of heat transfer varies with time. While the thermal conductivity of the suspension is improved due to the rise of the nano-additives concentration, its viscosity also increases. Thus, the viscous forces that hinder the flow are intensified, mainly when the cavity is in a descending motion.
- Increasing the Rayleigh number, indicating the relative dominance of the buoyancy forces over viscous ones, enhances heat transfer. It also improves the heating effectiveness. Similarly, the intensity of heat transfer and the heating effectiveness are improved when the vibration Rayleigh number is raised, pointing out the contribution of the vibration intensity to heat transfer in the cavity.

Declaration of Competing Interest

The authors clarify that there is no conflict of interest for report.

Acknowledgements

This work was supported by computational resources provided by the Australian Government through University of New South Wales under the National Computational Merit Allocation Scheme.

References

[1] Z.S. Kareem, M.N. Mohd Jaafar, T.M. Lazim, S. Abdullah, A.F. AbdulWahid, Heat transfer enhancement in two-start spirally corrugated tube, Alexandr. Eng. J. 54 (3) (2015) 415–422.
[2] A. Dadvand, S. Hosseini, S. Aghebatandish, B.C. Khoo, Enhancement of heat and mass transfer in a microchannel via passive oscillation of a flexible vortex generator, Chem. Eng. Sci. 207 (2019) 556–580.
[3] S. Kumar, R.S. Amano, J.M. Lucci, Numerical simulations of heat transfer distribution of a two-pass square channel with V-rib turbulator and bleed holes, Heat Mass Transf. 49 (8) (2013) 1141–1158.
[4] C. Zhang, D. Wang, K. Ren, Y. Han, Y. Zhu, X. Peng, J. Deng, X. Zhang, A comparative review of self-rotating and stationary twisted tape inserts in heat exchanger, Renew. Sust. Energ. Rev. 53 (2016) 433–449.
[5] K. Anantha Kumar, V. Sugunamma, N. Sandeep, Influence of viscous dissipation on MHD flow of micropolar fluid over a slendering stretching surface with modified heat flux model, J. Therm. Anal. Calorim. 139 (6) (2020) 3661–3674.
[6] K. Anantha Kumar, V. Sugunamma, N. Sandeep, Effect of thermal radiation on MHD Casson fluid flow over an exponentially stretching curved sheet, J. Therm. Anal. Calorim. 140 (5) (2020) 2377–2385.
[7] K.A. Kumar, V. Sugunamma, N. Sandeep, M.T. Mustafa, Simultaneous solutions for first order and second order slips on micropolar fluid flow across a convective surface in the presence of Lorentz force and variable heat source/sink, Sci. Rep. 9 (1) (2019) 14706.

[8] K. Anantha Kumar, V. Sugunamma, N. Sandeep, Physical aspects on unsteady MHD-free convective stagnation point flow of micropolar fluid over a stretching surface, Heat Transf. Asian Res. 48 (8) (2019) 3968–3985.
[9] K.A. Kumar, V. Sugunamma, N. Sandeep, A non-Fourier heat flux model for magnetohydrodynamic micropolar liquid flow across a coagulated sheet, Heat Transf. Asian Res. 48 (7) (2019) 2819–2843.
[10] A. Kumar, V. Sugunamma, N. Sandeep, Impact of non-linear radiation on MHD non-aligned stagnation point flow of micropolar fluid over a convective surface, J. Non-Equilibr. Thermodyn. 43 (4) (2018) 327–345.
[11] A. Kumar, V. Sugunamma, N. Sandeep, Numerical exploration of MHD radiative micropolar liquid flow driven by stretching sheet with primary slip: a comparative study, J. Non-Equilibr. Thermodyn. 44 (2) (2019) 101–122.
[12] B. Ramadevi, K. Anantha Kumar, V. Sugunamma, J.V. Ramana Reddy, N. Sandeep, Magnetohydrodynamic mixed convective flow of micropolar fluid past a stretching surface using modified Fourier's heat flux model, J. Therm. Anal. Calorim. 139 (2) (2020) 1379–1393.
[13] F. Wu, G. Wang, W. Zhou, Buoyancy induced convection in a porous cavity with sinusoidally and partially thermally active sidewalls under local thermal non-equilibrium condition, Int. Commun. Heat Mass Transf. 75 (2016) 100–114.
[14] D. Wen, G. Lin, S. Vafaei, K. Zhang, Review of nanofluids for heat transfer applications, Particuology 7 (2) (2009) 141–150.
[15] A.E. Bergles, Recent developments in enhanced heat transfer, Heat Mass Transf. 47 (8) (2011) 1001.
[16] M. Legay, N. Gondrexon, S. Le Person, P. Boldo, A. Bontemps, Enhancement of heat transfer by ultrasound: review and recent advances, Int. J. Chem. Eng. 2011 (2011) 670108.
[17] A.M. Rishem, M.H. Al-Hafidh, The effect of longitudinal vibration on laminar forced convection heat transfer in a horizontal tube, J. Eng. 12 (3) (2006) 863–879.
[18] Y. Lin, B. Farouk, Heat transfer in a rectangular chamber with differentially heated horizontal walls: effects of a vibrating sidewall, Int. J. Heat Mass Transf. 51 (11) (2008) 3179–3189.
[19] Y. Yao, X. Zhang, Y. Guo, Experimental Study on Heat Transfer Enhancement of Water-Water Shell-and-Tube Heat Exchanger Assisted by Power Ultrasonic, 2010.
[20] R.K. Gould, Heat transfer across a solid-liquid Interface in the presence of acoustic streaming, J. Acoustic. Soc. Am. 40 (1) (1966) 219–225.
[21] H. Shokouhmand, F. Sangtarash, The effect of flexible tube vibration on pressure drop and heat transfer in heat exchangers considering viscous dissipation effects, Heat Mass Transf. 44 (12) (2008) 1435–1445.
[22] D.W. Zhou, Heat transfer enhancement of copper nanofluid with acoustic cavitation, Int. J. Heat Mass Transf. 47 (14) (2004) 3109–3117.
[23] L. Zhang, J. Lv, M. Bai, D. Guo, Effect of vibration on forced convection heat transfer for SiO2–water nanofluids, Heat Transf. Eng. 36 (5) (2015) 452–461.
[24] N.A.C. Sidik, I.M. Adamu, M.M. Jamil, Preparation methods and thermal performance of hybrid nanofluids, J. Adv. Rev. Sci. Res. 24 (2016) 13–23.
[25] N. Jha, S. Ramaprabhu, Thermal conductivity studies of metal dispersed multiwalled carbon nanotubes in water and ethylene glycol based nanofluids, J. Appl. Phys. 106 (8) (2009), 084317.
[26] C.J. Ho, J.B. Huang, P.S. Tsai, Y.M. Yang, On laminar convective cooling performance of hybrid water-based suspensions of Al2O3 nanoparticles and MEPCM particles in a circular tube, Int. J. Heat Mass Transf. 54 (11) (2011) 2397–2407.
[27] S. Suresh, K.P. Venkitaraj, P. Selvakumar, M. Chandrasekar, Synthesis of Al2O3–cu/water hybrid nanofluids using two step method and its thermo physical properties, Colloids Surf. A Physicochem. Eng. Asp. 388 (1) (2011) 41–48.
[28] H.H. Balla, S. Abdullah, W. MohdFaizal, R. Zulkifli, K. Sopian, Numerical study of the enhancement of heat transfer for hybrid CuO-cu nanofluids flowing in a circular pipe, J. Oleo Sci. 62 (7) (2013) 533–539.
[29] A. Shahsavar, M. Saghafian, M.R. Salimpour, M.B. Shafii, Experimental investigation on laminar forced convective heat transfer of ferrofluid loaded with carbon nanotubes under constant and alternating magnetic fields, Exp. Thermal Fluid Sci. 76 (2016) 1–11.
[30] M. Goharkhah, A. Salarian, M. Ashjaee, M. Shahabadi, Convective heat transfer characteristics of magnetite nanofluid under the influence of constant and alternating magnetic field, Powder Technol. 274 (2015) 258–267.
[31] M. Lajvardi, J. Moghimi-Rad, I. Hadi, A. Gavili, T. Dallali Isfahani, F. Zabihi, J. Sabbaghzadeh, Experimental investigation for enhanced ferrofluid heat transfer under magnetic field effect, J. Magn. Magn. Mater. 322 (21) (2010) 3508–3513.
[32] R. Azizian, E. Doroodchi, T. McKrell, J. Buongiorno, L.W. Hu, B. Moghtaderi, Effect of magnetic field on laminar convective heat transfer of magnetite nanofluids, Int. J. Heat Mass Transf. 68 (2014) 94–109.
[33] D. Jehad, G. Hashim, Numerical prediction of forced convective heat transfer and friction factor of turbulent nanofluid flow through straight channels, J. Adv. Res. Fluid Mech. Therm. Sci 8 (1) (2015) 1–10.
[34] Y. Lee, The use of nanofluids in domestic water heat exchanger, J. Adv. Res. Appl. Mech 3 (1) (2014) 9–24.
[35] S. Abubakar, N.C. Sidik, Numerical prediction of laminar nanofluid flow in rectangular microchannel heat sink, J. Adv. Res. Fluid Mech. Therm. Sci 7 (1) (2015) 29–38.
[36] R. Nimmagadda, K. Venkatasubbaiah, Conjugate heat transfer analysis of micro-channel using novel hybrid nanofluids, Europ. J. Mech. B Fluids 52 (2015) 19–27.
[37] M.H. Esfe, A.A.A. Arani, M. Rezaie, W.-M. Yan, A. Karimipour, Experimental determination of thermal conductivity and dynamic viscosity of Ag–MgO/water hybrid nanofluid, Int. Commun. Heat Mass Transf. 66 (2015) 189–195.
[38] Q. Sun, I. Pop, Free convection in a triangle cavity filled with a porous medium saturated with nanofluids with flush mounted heater on the wall, Int. J. Therm. Sci. 50 (11) (2011) 2141–2153.
[39] J.N. Reddy, D.K. Gartling, The Finite Element Method in Heat Transfer and Fluid Dynamics, CRC Press, 2010.
[40] O. Zienkiewicz, R. Taylor, P. Nithiarasu, The Finite Element Method, Vol. 3 Fluid Dynamics, Butterworth-Heinemann, Oxford, 2005.
[41] W.-S. Fu, W.-J. Shieh, Transient thermal convection in an enclosure induced simultaneously by gravity and vibration, Int. J. Heat Mass Transf. 36 (2) (1993) 437–452.
[42] F. Corvaro, M. Paroncini, An experimental study of natural convection in a differentially heated cavity through a 2D-PIV system, Int. J. Heat Mass Transf. 52 (1) (2009) 355–365.
[43] K. Kahveci, Buoyancy driven heat transfer of nanofluids in a tilted enclosure, J. Heat Transf. 132 (6) (2010), 062501.
[44] K. Kahveci, Buoyancy driven heat transfer of nanofluids in a tilted enclosure, J. Heat Transf. 132 (6) (2010).